journal

Reprinted from the Journal of the American Ceramic Society, Vol. 76, No. 9, September 1993

J. Am. Ceram. Soc., 76 [9] 2235–40 (1993)

Model for Toughness Curves in Two-Phase Ceramics: I, Basic Fracture Mechanics

Brian R. Lawn,* Nitin P. Padture,*,† Linda M. Braun,* and Stephen J. Bennison*,‡

Ceramics Division, Materials Science and Engineering Laboratory, National Institute of Standards and Technology, Gaithersburg, Maryland 20899

A fracture mechanics model is presented for the toughening of ceramics by bridging from second-phase particles, resulting in toughness curve (*T*-curve) behavior. It is assumed that the second-phase particles are in a state of residual thermal expansion dilatational mismatch relative to the matrix. In the long-crack region, these stresses augment frictional sliding stresses at the interphase boundaries, enhancing the crack resistance; in the short-crack region, the same stresses drive the crack, diminishing the crack resistance. The principal manifestation of these countervailing influences is a reduced sensitivity of strength to initial flaw size, i.e., an increased flaw tolerance. In seeking to incorporate these key physical elements, our model opts for mathematical simplicity by assuming uniformly distributed stresses in two bridging domains: in the first, at small crack-wall separations, a constant opening stress; in the second, at larger separations, a constant closing stress. The uniform crack-plane distributions allow for simple closed-form solutions of the crack *K*-field equations, and thence an analytical formulation for the *T*-curve. Indentation–strength data on a "reference" Al_2O_3/Al_2TiO_5 ceramic composite are used to demonstrate the main theoretical predictions and to calibrate essential parameters in the *T*-curve formulation. The utility of the model as a route to microstructural design is addressed in Part II.

I. Introduction

It is now acknowledged that the toughness of monophase ceramics can exhibit a crack-size dependence, the so-called *toughness curve* (*T*-curve) or *resistance curve* (*R*-curve).[1–7] In nontransforming ceramics the *T*-curve is attributable principally to a mechanism of "bridging" by frictional grain slideout, greatly enhanced in noncubic materials by thermal expansion anisotropy stresses.[6] A characteristic of such ceramics is "flaw tolerance",[3–5,7–17] i.e., a diminished dependence of strength σ_F on initial flaw size c_f, relative to traditional "Griffith" behavior ($\sigma_F \propto c_f^{-1/2}$). Flaw tolerance in monophase ceramics may be enhanced by scaling up the grain size.[18] Beyond a *limiting* grain size, however, microcracking occurs spontaneously through the bulk material, with a consequent degradation of strength. These characteristics imply an element of compromise in materials design, e.g., increased strength in the long-crack region at the potential expense of bulk microcracking and reduced wear resistance in the short-crack region.[19]

Additions of a second phase can augment the *T*-curve behavior, well beyond any "law of mixtures," by enhancing the effectiveness and density of bridges. This is the underlying philosophy of reinforced composites. An important element in the materials design is the control of volume fraction and particle size, as well as internal residual stress. Increasing the volume fraction enhances the density of active bridges; increasing the particle size enhances the scale of these bridges. It follows that, with a proper understanding of these factors, one may better tailor microstructures for specified structural applications.

In the present study we extend the theory of grain bridging from monophase ceramics to two-phase ceramics, with special reference to alumina-matrix composites containing aluminum titanate particulate reinforcement.[6,20,21] Aluminum titanate is chosen as a second phase because of its large thermal expansion mismatch relative to alumina, so as to maximize the intensity of internal residual stresses at the bridge sites. Our endeavor is to establish a simple fracture mechanics model for the *T*-curve in this class of ceramic. In emphasizing simplicity, we are prepared to sacrifice mathematical rigor in the model, but not at the expense of physical essentials. Thus, we retain our capacity to incorporate basic microstructural elements, volume fraction, particle size, and residual stress, as governing microstructural variables in the description. Experimental indentation–strength data on the composite materials will be used to illustrate the versatility of the model, most notably in the short-crack region.

The study is presented in two parts. In Part I we outline the basic theory and analyze the principal features of the *T*-curve for our composite material. In Part II we investigate the effects of microstructural variables on the *T*-curve and associated flaw tolerance, with consideration of restrictions imposed by bulk microcracking limits.

II. Theoretical *K*-Field Analysis

We begin by deriving *K*-field relations for cracks in an otherwise homogeneous ceramic matrix with bridging second-phase particles. In developing these relations we shall borrow from earlier theoretical treatments for monophase ceramics[13] and fiber-reinforced composites,[22] but with the simplification of continuous and uniformly distributed (Barenblatt–Dugdale) bridging stresses over the crack interface. The analysis will be used to determine *T*-curve and strength formalisms for materials with indentation short cracks.

(1) *Stress-Separation Function*

Consider two surfaces bridged by second-phase particles over a separation $2u$ (Fig. 1). We concern ourselves with crack areas large relative to that occupied by a single particle, so that a distribution of *discrete* force–separation functions may be replaced by a *continuous* stress–separation function, $s(u)$, say. We shall regard $s(u)$ as a positive quantity (shielding) when it acts to close the interface; this convention is consistent with an enhanced long-crack toughness. At the same time, we recognize the need to allow for the possibility of negative $s(u)$ (anti-shielding) at small separations, so as to allow for microcracking in the short-crack region.

D. K. Shetty—contributing editor

Manuscript No. 195174. Received October 27, 1992; approved May 28, 1993.
Supported by the U.S. Air Force Office of Scientific Research and E. I. duPont Nemours and Company Inc.
*Member, American Ceramic Society.
†Guest Scientist, from Department of Materials Science and Engineering, Lehigh University, Bethlehem, PA 18015.
‡Now at Experimental Station, E. I. DuPont Nemours and Company, Wilmington, DE 19880–0356.

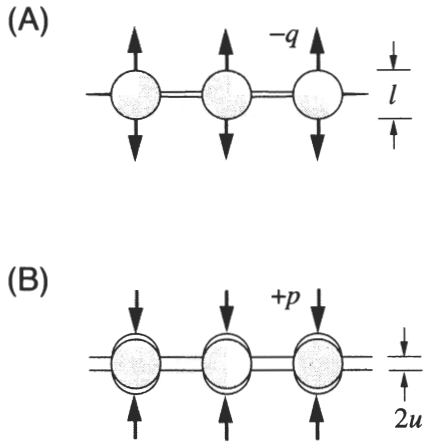

Fig. 1. Schematic diagram depicting interaction of second-phase particles with separating matrix walls. (A) Crack opening at small separations, due to residual outward pressure from compressed particles. (B) Bridging at large separations, from frictional tractions at sliding grain-matrix interphase boundaries.

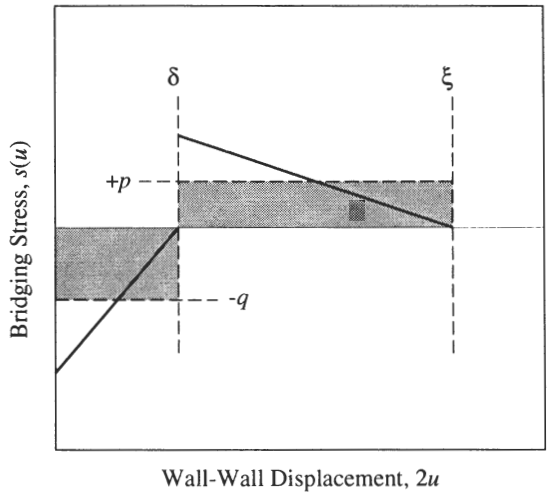

Fig. 2. Stress–separation function, $s(u)$, for system in Fig. 1. Shaded areas indicate approximations of uniform stress $s = +p$ and $s = -q$ in the two domains. (Positive sign denotes *closure* bridging stress.)

We therefore assume the bridging particles to exist in a state of residual compressive stress at the uncracked interface, so that they initially exert opening stresses on the matrix walls. As the walls separate, these opening stresses relax. At the same time, the particles debond from the matrix. At larger separations the particles begin to slide out of the constraining matrix but are restrained at those interphase boundary facets where the thermal expansion mismatch stresses are compressive. Resistance to sliding pullout then arises principally from Coulombic frictional tractions.[13] For simplicity, we assume that the transition to frictional sliding occurs when the precompressed springs are *just* relaxed, and neglect any resistance stresses due to debonding.

The function $s(u)$ at small u is then determined as the opening stress exerted on the matrix over the section area of a single particle, relative to the interface area occupied by that particle:

$$s(u) = -V_f(1 - V_f)(1 - 2u/\delta)\sigma_R \qquad (0 \le 2u \le \delta) \qquad (1a)$$

where V_f is the volume fraction, σ_R is the thermal expansion mismatch stress at the interphase boundary, and δ is the separation at which the residual elastic stresses are relaxed. (The factor $1 - V_f$ is to allow for a reduction in available matrix volume at increasing V_f, with $V_f < 0.5$.) Similarly, $s(u)$ at large u is determined as the closing stress exerted on the matrix over the interphase frictional contact area of the particle, again relative to the fractional interface area:[13]

$$s(u) = +V_f(1 - V_f)(1 - 2u/\xi)\eta\xi\mu\sigma_R/l \qquad (\delta \le 2u \le \xi) \qquad (1b)$$

where l is the particle diameter, η is a particle–matrix perimeter/area factor relative to l at the crack plane,[13] μ is the coefficient of sliding friction, and ξ is the separation at which the particle disengages ($\delta << \xi$, usually). The composite $s(u)$ function of Eq. (1) is plotted in Fig. 2.

While acknowledging the *physical* sensibility of the *linear* ("tail") stresses in the $s(u)$ function,[8,13] it is nevertheless *mathematically* expedient to replace these by *uniform* stresses over the pertinent bridging zones, as indicated in Fig. 1. Let us therefore define "averaged" values p and q over the two bridging zones:

$$s(u) = -q = -\frac{1}{2}V_f(1 - V_f)\sigma_R \qquad (0 \le 2u \le \delta) \qquad (2a)$$

$$s(u) = +p = \frac{1}{2}\eta\mu\varepsilon_\xi V_f(1 - V_f)\sigma_R \qquad (\delta \le 2u \le \xi) \qquad (2b)$$

with conjugate size-independent strain terms

$$\varepsilon_\delta = \delta/l \qquad (3a)$$

$$\varepsilon_\xi = \xi/l \qquad (3b)$$

(2) K-Field and T-Curve

Now consider the stress–separation function of Eq. (2) in the context of pennylike short cracks, to simulate the evolution of flaws (natural or artificially induced) under the action of an externally applied tensile stress. We assume that in their critical growth stages to failure the cracks traverse a large number of particles, so that we may be justified in using the *continuous* stress function $s(u)$ to describe the ensuing strength characteristics. (This assumption will be examined when we compute the cohesion-zone dimensions for our composite material later.)

Accordingly, the stress distribution along the coordinate r of a penny crack (Fig. 3) is

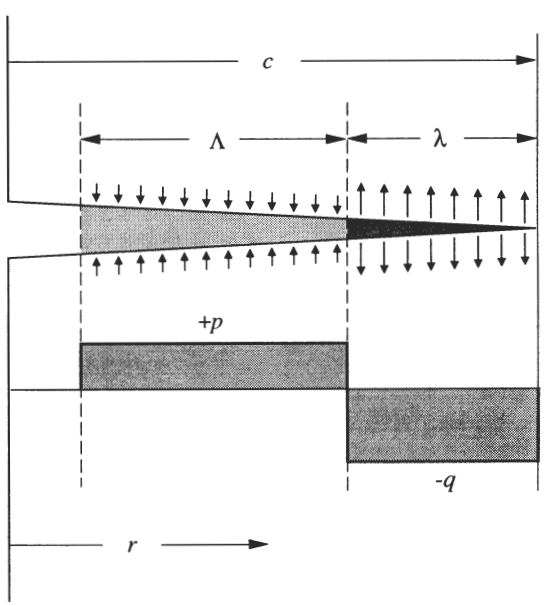

Fig. 3. Equivalent stress distribution, $s(r)$, for bridged crack.

$$s(r) = -q \qquad (c - \lambda \le r \le c) \tag{4a}$$

$$s(r) = p \qquad (c - \Lambda - \lambda \le r \le c - \lambda) \tag{4b}$$

with c the crack radius. The bridging zone dimensions λ and Λ scale with the crack-opening displacements δ and ξ of Fig. 1 via some crack profile relation (with $\lambda << \Lambda$, usually). In part I, the need for knowledge of the profile may be avoided, by simplistically treating λ and Λ as adjustable parameters; this will not be so in Part II, when we consider the role of microstructural variables.

The "crack-tip" K-field, K_*, for an equilibrium crack under applied stress σ_A in a bridging material contains a microstructural component, K_μ:

$$K_*(c) = \psi\sigma_A c^{1/2} + K_\mu(c) = T_0 \tag{5}$$

with T_0 the intrinsic toughness of the matrix material (grain boundary toughness in the case of intergranular fracture). Putting $-K_\mu = T_\mu$ (so that a true *shielding* term appears as a *positive* contribution to the toughness), we may write the "global" K-field as

$$K_A(c) = \psi\sigma_A c^{1/2} = T_0 - K_\mu(c)$$
$$= T_0 + T_\mu(c) = T(c) \tag{6}$$

which defines the toughness curve, or T-curve, $T(c)$.

To determine $T_\mu(c)$, we integrate the bridging stresses of Eq. (4) over the entire crack area, using the conventional Green's function expression for pennylike cracks:[23]

$$T_\mu(c) = 2\alpha/(\pi c)^{1/2}\int_0^c rs(r)\mathrm{d}r/(c^2 - r^2)^{1/2} \tag{7}$$

where α is a geometrical coefficient to allow for interactions with specimen and crack-neighbor free surfaces. For indentation radial cracks, one generally defines a coefficient $\psi = 2\alpha/\pi^{1/2}$, to allow for *half*-penny geometry, any ensuing distortions into elliptical fronts, and perturbations from orthogonal radial and lateral cracks. Integration within three different regions of crack size gives the microstructural function

$$T_\mu(c) = -\psi q c^{1/2} \qquad (0 \le c \le \lambda) \tag{8a}$$

$$T_\mu(c) = \psi q c^{1/2}\{1 - [1 - (1 - \lambda/c)^2]^{1/2}\}$$
$$- \psi q c^{1/2}[1 - (1 - \lambda/c)^2]^{1/2}$$
$$(\lambda \le c \le \Lambda + \lambda) \tag{8b}$$

$$T_\mu(c) = \psi p c^{1/2}\{[1 - (1 - \Lambda/c - \lambda/c)^2]^{1/2}$$
$$- [1 - (1 - \lambda/c)^2]^{1/2}\}$$
$$- \psi q c^{1/2}[1 - (1 - \lambda/c)^2]^{1/2}$$
$$(\Lambda + \lambda \le c) \tag{8c}$$

The ensuing $T(c)$ function in Eq. (6) may be usefully simplified in certain regions of c by making some reasonable approximations. In the limit of a very small tensile zone, λ becomes independent of c ("small-zone," or "Barenblatt," approximation), and Eq. 8(b) results in a T-curve that is linear in $c^{1/2}$:

$$T(c) = T_0 - \psi(p + q)(2\lambda)^{1/2} + \psi p c^{1/2}$$
$$(\lambda << c \le \Lambda + \lambda) \tag{9}$$

In the limit of very long cracks, Eq. (8c) results in

$$T(c) = T_0 - \psi(p + q)(2\lambda)^{1/2} + \psi p(2\Lambda)^{1/2}$$
$$(\Lambda + \lambda << c) \tag{10}$$

corresponding to the plateau toughness.

(3) Indentation–Strength

Now let us extend the analysis to Vickers indentation flaws, so that we may use indentation–strength data to evaluate the T-curve parameters in Eqs. (8–10) objectively for our test material (Sect. III).

It is necessary now to include one further term in our formulation, to allow for the residual K-field associated with the irreversible contact deformation at indentation load P. The equilibrium crack-tip K-field relation of Eq. (5) is modified to[13,24]

$$K_*(c) = \psi\sigma_A c^{1/2} + \chi P/c^{3/2} + K_\mu(c) = T_0 \tag{11}$$

corresponding to a global K-field

$$K'_A(c) = \psi\sigma_A c^{1/2} + \chi P/c^{3/2}$$
$$= T_0 - K_\mu(c) = T_0 + T_\mu(c) = T(c) \tag{12}$$

The residual-contact term provides additional stabilization to the crack. The inert strength for indentation flaws is the configuration $\sigma_A = \sigma_M$, $c = c_M$ at which the transposed function

$$\sigma_A(c) = (1/\psi c^{1/2})[T(c) - \chi P/c^{3/2}] \tag{13}$$

from Eq. (12) satisfies the requirement $\mathrm{d}\sigma_A(c)/\mathrm{d}c = 0$ for a maximum, corresponding to the "tangency condition"

$$\mathrm{d}K'_A(c)/\mathrm{d}c = \mathrm{d}T(c)/\mathrm{d}c \tag{14}$$

in a conventional T-curve construction.[25]

Equation (13) is not readily solved analytically for σ_M, c_M using the general $T_\mu(c)$ relations in Eqs. (6) and (8). However, an exact solution *is* obtainable in the region $\lambda << c \le \Lambda + \lambda$, using Eq. (9). If we write $\sigma'_A = \sigma_A - p$, $T'_0 = T_0 - \psi(p + q)(2\lambda)^{1/2}$, Eq. (11) then reduces to the exact same form as the standard relation for materials with single-valued toughness,[13,24]

$$K_*(c) = \psi\sigma'_A c^{1/2} + \chi P/c^{3/2} = T'_0 \tag{15}$$

Solving for the instability configuration in Eq. (14), or by direct inspection of the standard solutions for such homogeneous materials,[26,27] one obtains

$$c_M = \{4\chi P/[T_0 - \psi(p + q)(2\lambda)^{1/2}]\}^{2/3} \tag{16a}$$

$$\sigma_M = p + 3[T_0 - \psi(p + q)(2\lambda)^{1/2}]^{4/3}/4\psi(4\chi P)^{1/3} \tag{16b}$$

We shall assert that, because of the long precursor extensions from initial size c_0 to final size c_M for indentation cracks, the specification $\lambda << c \le \Lambda + \lambda$ poses no severe restriction to the validity of Eq. (16). Note that for large P the strength is enhanced relative to the homogeneous matrix material ($p = 0 = q$), because of the lower-limiting stress p; at small P the strength is reduced, because of the diminished effective toughness T'_0 (square bracket term). Hence, the formalism embodies the essential quality of flaw tolerance.

III. Fits to Data for Two-Phase Al_2O_3/Al_2TiO_5 Composite

(1) Experimental Procedure

We illustrate the above formulation with indentation–strength data from a fine-grain alumina matrix reinforced by homogeneously distributed aluminum titanate particles (Al_2O_3/Al_2TiO_5). The fabrication procedure for this composite material has been described elsewhere.[20,21,28,29] Materials were fabricated with a starting grain size <2 μm, and the particles subsequently grown by a prescribed aging heat treatment.[21] Densities were measured using the Archimedes method, >98% in all cases, and the particle size by a lineal intercept method.[21] In Part I we focus on a reference composition with volume fraction V_f =

0.20 and mean second-phase particle size $l = 4.0$ μm. The alumina grain size is <7 μm, so that there is negligible contribution to the T-curve from the matrix itself.[18] A micrograph of the microstructure is shown in Fig. 4.

Additional batches of the alumina-matrix material were also fabricated with different values of V_f and l, for consideration in the scond part of this study (see Part II).

Specimens for strength testing were prepared as disks, 20-mm diameter and 2.5-mm thickness, with one surface polished to better than 1 μm. A Vickers indentation was made at the center of each polished surface, at prescribed load P, and covered with a drop of silicone oil. The disks were then broken in biaxial flexure, indentations on the tensile side, with 4-mm-diameter flat loading on a 15-mm-diameter three-ball support. These tests were run in "fast" loading (<10 ms failure time), to ensure "inert" conditions. Post-mortem examinations were made of all broken specimens to confirm failure initiation from the indentation sites.

The indentation–strength, $\sigma_M(P)$, results are plotted as the data points in Fig. 5. Error bars are standard deviation bounds for 4–6 tests at each indentation load.

(2) Evaluation of T-Curve Parameters from Indentation–Strength Data

Our approach is to evaluate the short-crack T-curve for our alumina-based composite from the $\sigma_M(P)$ data in Fig. 5, following a procedure developed in an earlier study.[24] Using coefficients $\psi = 0.77$ and $\chi = 0.076$ calibrated on a fine-grain alumina reference material in that earlier study, we first generate $K'_A(c)$ functions (Eq. (12)) for each of the $\sigma_M(P)$ data points. The $T(c)$ function is then determined as the "envelope of tangency points" (Eqs. (12) and (14)) fitted to the family of $K'_A(c)$ functions, inserting a calibrated value of $T_0 = 2.75$ MPa·m$^{1/2}$ from the earlier study in Eq. (6) and adjusting the microstructural parameters in Eq. (8).

We do this in Fig. 6, as toughness T against crack-size quantity $c^{1/2}$. In this plot the $K'_A(c)$ functions are shown as the inverted solid curves. The heavy curve is a fit of the $T(c)$ function in Eqs. (6) and (8). To obtain this fit, we first used a least-squares procedure to evaluate the following parameters for the "reference state" at $V_f = 0.20$, $l = 4.0$ μm:

$$p = 325 \text{ MPa} \tag{17a}$$

$$(p + q)(2\lambda)^{1/2} = 3.51 \text{ MPa·m}^{1/2} \tag{17b}$$

$$\Lambda = 180 \text{ μm} \tag{17c}$$

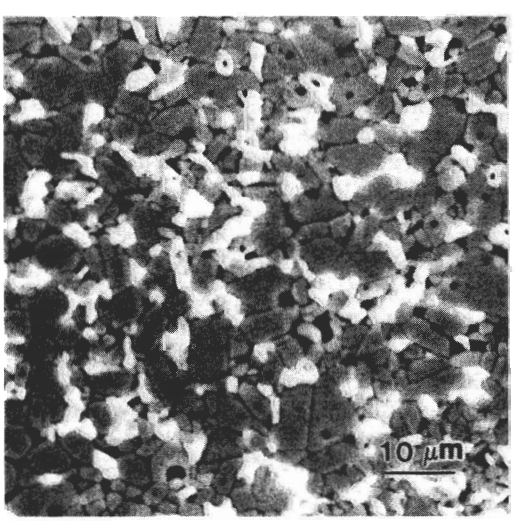

Fig. 4. Scanning electron micrograph showing Al_2TiO_5 particles ($V_f = 0.20$, white phase) in Al_2O_3 matrix (dark phase), for reference composite.

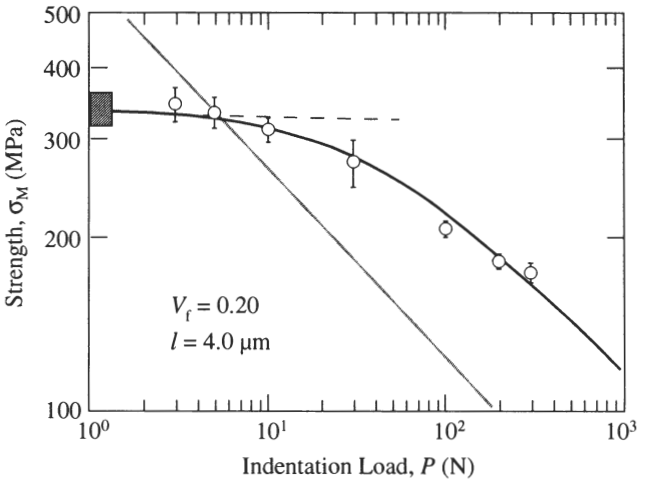

Fig. 5. Indentation–strength plot for reference Al_2O_3/Al_2TiO_5 composite ($V_f = 0.20$, $l = 4.0$ μm). Data points are means and standard deviations of 4–6 tests per load. Solid curve is generated theoretically from the condition $d\sigma_A(c)/dc = 0$ in Eq. (13) (using microstructural parameters evaluated from the T-curve fit in Fig. 6). Dashed curve is "plateau" approximation from Eq. (16b). Shaded line of slope $-1/3$ represents indentation–strength results for base fine-grain matrix alumina.

Recall from Eq. (9) that these parameters completely determine an approximate "linear" T–$c^{1/2}$ representation of $T(c)$, with slope p and T-axis intercept $T_0 - \psi(p + q)(2\lambda)^{1/2}$; this representation is included as the inclined dashed curve in Fig. 6. Observe the continuous rollover in the complete $T(c)$ function to saturation at $c >> \Lambda + \lambda$, as the fully developed bridging zone begins to translate with the crack.

Since the strength data in Fig. 6 do not extend down into the region $c < \lambda$, we need additional information to determine the full set of microstructural parameters in the T-curve function. Precise values of the remaining parameters are not crucial to our treatment at this juncture, so we take

$$\lambda = 7.0 \text{ μm} \tag{18a}$$

$$q = 613 \text{ MPa} \tag{18b}$$

to match estimates of the short-crack size ($c \approx 2\lambda$) at first microcracking in Al_2O_3/Al_2TiO_5 composites with scaled-up microstructures (see Part II). Observe also the minimum at

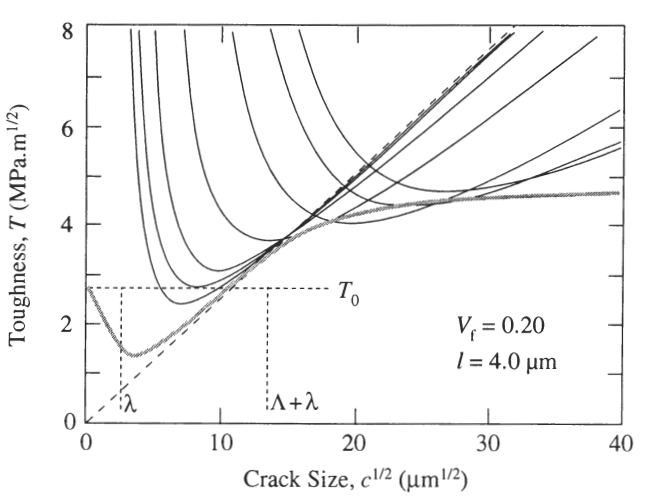

Fig. 6. T-curve constructions for reference Al_2O_3/Al_2TiO_5 composite. Family of inverted curves represents $K'_A(c)$ functions in Eq. (12) evaluated for (σ_M,P) data points in Fig. 5. Shaded curve is fitted envelope $T(c)$ function from Eqs. (6) and (8).

small c, signifying a degradation in toughness at $c < 2\lambda$ from the initial crack-opening action of second-phase particles.

With the estimates $\eta \approx 4$ (rectangular or circular cross-section particle) and $\varepsilon_\xi \approx 0.050$ (Sect. III(1)), we may use Eq. (2) to evaluate the composite material quantities

$$\sigma_R = 7.7 \text{ GPa} \tag{19a}$$

$$\mu \approx 2.7 \tag{19b}$$

Given the microstructural T-curve parameters in Eqs. (17) and (18), complete theoretical indentation–strength, $\sigma_M(P)$, curves may now be regenerated by seeking extremum solutions of Eq. (13). Figure 5 includes curves thus regenerated, using the full $T(c)$ function in Eqs. (6) and (8) (solid curve) and the "linear" T–$c^{1/2}$ approximation in Eq. (9) (dashed curve). The intersection of the solid curve through the data reinforces the validity of our fitting procedure in Fig. 6.

IV. Discussion

The above analysis allows us to analyze the T-curve response of two-phase ceramics in the short-crack region using indentation–strength data. A major feature of the analysis is its relative *simplicity*. Thus, although discrete microstructural parameters are used in defining the underlying bridging stress–separation function, Eqs. (1) and (2), we are nevertheless able to regard the same bridging stresses as *continuously* distributed along the crack plane, Eq. (4). The assumption of *uniform* stresses within the bridging zones (Figs. 1 and 2) allows for analytical solutions of the K-field integral equations. The exercise is thereby reduced to something akin to a Barenblatt–Dugdale crack problem. Moreover, by calibrating λ and Λ in Eqs. (8–10) directly from experimental data, our solutions can be determined *without at this stage specifying any crack-opening displacement relation* (see, however, Part II). In this context we may note that the estimated dimension $\lambda = 7.0$ μm (Sec. III(2)) is comparable to the Al_2TiO_5 interparticle separation in Fig. 4, so the continuum approximation is open to some question in the crack-size domain to the left of the $T(c)$ minimum in Fig. 6.

One of the advantages of the present model is the clear way it identifies essential T-curve and associated flaw tolerance characteristics with specific elements of the microstructure. Thus we note in Eq. (9) that the *slope* of the T-curve is proportional to the bridging stress p. From Eq. (2b), this stress increases monotonically with volume fraction V_f and residual stress σ_R. We also note in Eq. (9) that the *scale* of the T-curve is limited by the bridging zone length Λ. This dimension increases with particle size l (Part II). Hence we might expect to be able to enhance the relatively modest T-curve and flaw tolerance characteristics for our material in Figs. 5 and 6 by appropriately altering the microstructure. As we shall see in Part II, such potential enhancements are ultimately limited by the onset of general microcracking.

Our simple model is not without its limitations. Replacing the tail-dominated stress–separation functions in Fig. 1 by the uniform stresses p and q has inevitable consequences in the predicted shape of the T-curve. Nevertheless, our description contains the essence of microstructural scaling and internal stress influences, and will not affect the general physical conclusions drawn in either Parts I or II of this study.

Useful estimates of the controlling microstructural parameters emerge from the data fits in Figs. 5 and 6. The residual stress $\sigma_R \approx 7.7$ GPa (Eq. (19a)) is large but is of the order of computed thermal expansion anisotropy stresses for the Al_2O_3/Al_2TiO_5 system.[21] The friction coefficient $\mu \approx 2.7$ (Eq. (19b)) is also high but is nevertheless of the same order as that obtained in an earlier bridging analysis for pure alumina[13] and is not unreasonable for sliding contacts at *pristine* (freshly debonded) surfaces.[30]

There are interesting implications in the analysis concerning the stability of flaws that evolve through the residual bridging K-field in their initial state (cf. flaws with *no* residual K-field $\chi P/c^{3/2}$ in Eq. (11)), in response to an applied stress σ_A. The appropriate $K_A(c)$ function is a straight line through the origin of a T–$c^{1/2}$ plot, with slope $\psi\sigma_A$. For the particular Al_2O_3/Al_2TiO_5 composite in Fig. 6, the intercept of the extrapolated "linear" $T(c)$ function on the T-axis, $T_0 - \psi(p + q)(2\lambda)^{1/2}$ in Eq. (9), is *positive*. Hence in Fig. 6 the $K_A(c)$ line must always intersect the $T(c)$ curve with a slope $dK_A/d(c^{1/2}) > dT/d(c^{1/2})$. Under these conditions there is no T-curve "tangency" condition. This means that, whereas indentation flaws in our material show substantial precursor crack extension in a strength test, by virtue of the additional stabilizing influence of the residual contact K-field, natural flaws should propagate spontaneously to failure at their initial size, $c = c_f$ ("Griffith failure"). Our T-curve material in Fig. 6 does nevertheless exhibit a degree of flaw tolerance: the sensitivity of the strength σ_F for unindented specimens to c_f is manifestly reduced relative to a matrix base material at $T = T_0$.[3,5,7] Note that contrary to common practice $T(c)$ cannot, even in its oversimplified form of Eq. (9), be represented as a pure *power law*; the intercept term in the T-curve function is *vital* in determining the nature of the flaw response.

This last point will be made even more compellingly when we examine the effect of microstructural variations in Part II. The real power of the present model is that, once the controlling microstructural parameters for a given material system have been calibrated, in the manner of Sect. III(2), one may use the fracture mechanics to predict how the flaw tolerance characteristics vary with the microstructure. We will find that the T-axis intercept referred to above is depressed as volume fraction and particle size are increased, ultimately becoming negative and thereby altering the entire complexion of the flaw stability.

Acknowledgments: The authors acknowledge stimulating discussions with H. Cai, E. R. Fuller, Jr., and J. L. Runyan.

References

[1]H. Hübner and W. Jillek, "Subcritical Crack Extension and Crack Resistance in Polycrystalline Alumina," *J. Mater. Sci.*, **12,** 117–25 (1977).

[2]R. Knehans and R. Steinbrech, "Memory Effect of Crack Resistance during Slow Crack Growth in Notched Al_2O_3 Bend Specimens," *J. Mater. Sci. Lett.*, **1** [8] 327–29 (1982).

[3]B. R. Lawn and C. J. Fairbanks, "Toughness and Flaw Response in Non-Transforming Ceramics: Implications for NDE"; pp. 1023–32 in *Review of Progress in Quantitative NDE*, Vol. 6B. Edited by D. O. Thompson and D. E. Chimenti. Plenum Press, New York, 1987.

[4]R. F. Cook, C. J. Fairbanks, B. R. Lawn, and Y.-W. Mai, "Crack Resistance by Interfacial Bridging: Its Role in Determining Strength Characteristics," *J. Mater. Res.*, **2** [3] 345–56 (1987).

[5]S. J. Bennison and B. R. Lawn, "Flaw Tolerance in Ceramics with Rising Crack-Resistance Characteristics," *J. Mater. Sci.*, **24,** 3169–75 (1989).

[6]S. J. Bennison, J. Rödel, S. Lathabai, P. Chantikul, and B. R. Lawn, "Microstructure, Toughness Curves and Mechanical Properties of Alumina Ceramics"; pp. 209–33 in *Toughening Mechanisms in Quasi-Brittle Materials*. Edited by S. P. Shah. Kluwer Academic Publishers, Dordrecht, The Netherlands, 1991.

[7]S. J. Bennison, N. P. Padture, J. L. Runyan, and B. R. Lawn, "Flaw-Insensitive Ceramics," *Philos. Mag. Lett.*, **64** [4] 191–95 (1991).

[8]Y.-W. Mai and B. R. Lawn, "Crack-Interface Grain Bridging as a Fracture Resistance Mechanism in Ceramics: II, Theoretical Fracture Mechanics Model," *J. Am. Ceram. Soc.*, **70** [4] 289–94 (1987).

[9]P. L. Swanson, C. J. Fairbanks, B. R. Lawn, Y.-W. Mai, and B. J. Hockey, "Crack-Interface Grain Bridging as a Fracture Resistance Mechanism in Ceramics: I, Experimental Study on Alumina," *J. Am. Ceram. Soc.*, **70** [4] 279–89 (1987).

[10]A. Reichl and R. W. Steinbrech, "Determination of Crack Bridging Forces in Alumina," *J. Am. Ceram. Soc.*, **71** [6] C-299–C-301 (1988).

[11]P. L. Swanson, "Crack-Interface Traction: A Fracture-Resistance Mechanism in Brittle Polycrystals"; pp. 135–55 in Advances in Ceramics, Vol. 22, *Fractography of Glasses and Ceramics*. Edited by J. R. Varner and V. D. Frechette. American Ceramic Society, Westerville, OH, 1988.

[12]M. Sakai and R. C. Bradt, "The Crack Growth Resistance Curves of Non-Phase-Transforming Ceramics," *Nippon Seramikkusu Kyokai Gakujutsu Ronbunshi*, **96** [8] 801–809 (1988).

[13]S. J. Bennison and B. R. Lawn, "Role of Interfacial Grain-Bridging Sliding Friction in the Crack-Resistance and Strength Properties of Nontransforming Ceramics," *Acta Metall.*, **37** [10] 2659–71 (1989).

[14]E. K. Beauchamp and S. L. Monroe, "Effect of Crack-Interface Bridging on Subcritical Crack Growth in Ferrites," *J. Am. Ceram. Soc.*, **72,** 1179–84 (1989).

[15]G. Vekinis, M. F. Ashby, and P. W. R. Beaumont, "*R*-Curve Behaviour of Al_2O_3 Ceramics," *Acta Metall.*, **38** [6] 1151–62 (1990).

[16]J. Rödel, J. Kelly, and B. R. Lawn, "*In Situ* Measurements of Bridged Crack Interfaces in the SEM," *J. Am. Ceram. Soc.*, **73** [11] 3313–18 (1990).

[17]P. F. Becher, "Microstructural Design of Toughened Ceramics," *J. Am. Ceram. Soc.*, **74** [2] 255–69 (1991).

[18]P. Chantikul, S. J. Bennison, and B. R. Lawn, "Role of Grain Size in the Strength and *R*-Curve Properties of Alumina," *J. Am. Ceram. Soc.*, **73** [8] 2419–27 (1990).

[19]S.-J. Cho, B. J. Hockey, B. R. Lawn, and S. J. Bennison, "Grain-Size and *R*-Curve Effects in the Abrasive Wear of Alumina," *J. Am. Ceram. Soc.*, **72** [7] 1249–52 (1989).

[20]N. P. Padture, H. M. Chan, S. J. Bennison, J. L. Runyan, J. Rödel, and B. R. Lawn, "Flaw Tolerant Al_2O_3–Al_2TiO_5 Composites"; pp. 715–21 in Ceramic Transactions, Vol. 19, *Advanced Composite Materials*. Edited by M. D. Sacks. American Ceramic Society, Westerville, OH, 1991.

[21]J. L. Runyan and S. J. Bennison, "Fabrication of Flaw-Tolerant Aluminum–Titanate-Reinforced Alumina," *J. Eur. Ceram. Soc.*, **7**, 93–99 (1991).

[22]D. B. Marshall, B. N. Cox, and A. G. Evans, "The Mechanics of Matrix Cracking in Brittle-Matrix Fibre Composites," *Acta Metall.*, **23** [11] 2013–21 (1985).

[23]B. R. Lawn, *Fracture of Brittle Solids*. Cambridge University Press, Cambridge, U.K., 1993.

[24]L. M. Braun, S. J. Bennison, and B. R. Lawn, "Objective Evaluation of Short-Crack Toughness Curves Using Indentation Flaws: Case Study on Alumina-Based Ceramics," *J. Am. Ceram. Soc.*, **75** [11] 3049–57 (1992).

[25]Y.-W. Mai and B. R. Lawn, "Crack Stability and Toughness Characteristics in Brittle Materials," *Ann. Rev. Mater. Sci.*, **16,** 415–39 (1986).

[26]D. B. Marshall and B. R. Lawn, "Residual Stress Effects in Sharp-Contact Cracking: I. Indentation Fracture Mechanics," *J. Mater. Sci.*, **14** [8] 2001–12 (1979).

[27]D. B. Marshall, B. R. Lawn, and P. Chantikul, "Residual Stress Effects in Sharp-Contact Cracking: II. Strength Degradation," *J. Mater. Sci.*, **14** [9] 2225–35 (1979).

[28]N. P. Padture, S. J. Bennison, and H. M. Chan, "Flaw-Tolerance and Crack-Resistance Properties of Alumina–Aluminum Titanate Composites with Tailored Microstructures," *J. Am. Ceram. Soc.*, **76** [9] 2312–20 (1993).

[29]N. P. Padture, "Crack Resistance and Strength Properties of Some Alumina-Based Ceramics"; Ph.D. Dissertation. Lehigh University, Bethlehem, PA, 1991.

[30]X. Dong, S. Jahanmir, and S. M. Hsu, "Tribological Characteristics of α-Alumina at Elevated Temperatures," *J. Am. Ceram. Soc.*, **74** [5] 1036–44 (1991). □